SELECTIVE LOADING OF ORGANOFILIC Ag NANOPARTICLES IN PS/PMMA BLENDS

A Thesis Submitted to
the Graduate School of Engineering and Sciences of
İzmir Institute of Technology
in Partial Fulfillment of the Requirements for the Degree of

MASTER OF SCIENCE

in Material Science and Engineering

by
Şeyda TÜZÜNER

September 2014
İZMİR

We approve the thesis of **Şeyda TÜZÜNER**

Examining Committee Members:

_____

Prof. Dr. Mustafa M. DEMİR
Department of Material Science and Engineering,
İzmir Institute of Technology

_____

Assist. Prof. Dr. Yaşar AKDOĞAN
Department of Material Science and Engineering,
İzmir Institute of Technology

_____

Assoc. Prof . Dr. Mustafa EMRULLAHOĞLU
Department of Chemistry, İzmir Institute of Technology

19 September 2014

_____

Prof. Dr. Mustafa M. DEMİR
Supervisor, Department of Material Science and Engineering, İzmir Institute of Technology

_____

Asisst. Prof. Dr. Özgenç EBİL
Co-Advisor, Department of Chemical Engineering, İzmir Institute of Technology

_____

Prof. Dr. Mustafa M. DEMİR
Head of the Department of Material Science and Engineering

_____

Prof. Dr. R. Tuğrul SENGER
Dean of the Graduate School of Engineering and Science

ACKNOWLEDGEMENTS

I would like to thank my supervisor Prof. Dr. Mustafa M. DEMİR, for this supervision, guidance, endless support, and encouragement throughout my thesis study.

Also I would like to thank to my co-advisor Assist. Prof. Dr. Özgenç EBİL for his kind support, guidance for helping to me.

Special thanks to group members of Material Research Center, Işın ÖZÇELİK, Mine BAHÇECİ and Sinem HORTOĞLU for their scientific guidance, helping in analysis and valuable comments.

Besides, I would like to thank my friends; Assist. Prof. Dr. Nesrin HORZUM POLAT, Özlem KAP, Tuğba ISIK, Derya METE, Aslı ÇELİK, Anıl İNCEL, Alper İNAN and Emine BERBER for their helps and friendship during laboratory studies.

Finally, I am also grateful to my husband and my parents for their endless love, supports, patience and encouragements. I dedicate my thesis at first to my parents, Ali and Çağlayan BAĞCI and then to my husband (my sweet pie), İbrahim TÜZÜNER.

ABSTRACT

SELECTIVE LOADING OF ORGANOPHILIC Ag NANOPARTICLES IN PS/PMMA BLENDS

The association of nanoparticles with polymer blends offers significant features beyond the advantages of polymer composites prepared by single homopolymer. Since the blends undergo phase separation due to incompatibility of the constituent polymers into various internal structures, the particles can be segregated into one of the phases. Different location of the particles allows to develop novel microstructures; and thus, control over physical properties. In this study, Ag nanoparticles were prepared by reduction of $AgNO_3$ via $NaBH_4$. The particles were capped by cetyl ammonium bromide (CTAB) and were mixed with equimass blend of polystyrene (PS) and poly(methyl methacrylate) (PMMA) in tetrahydrofurane (THF). The solid content of blend solution was fixed at 2.5% w/v. The concentration of the particles with respect to polymer blend was at 0.7 wt %. The composite film was cast on glass slide. Surface feature of the composite films was examined by atomic force microscopy (AFM) and scanning electron microscopy (SEM). The surface of blend film without particles shows spherical pits with a size of 4.5 μm and rich in terms of PMMA. When particle size was small (diameter is around 20 nm), they preferentially located at the interface of the domains. The large particles with a diameter of 90 nm were found to locate in PMMA phase. Upon annealing of the composite film at 165 ˚C for 3 days, the particles move to the PS domains independent of the particle size and merely PS loaded composite is achieved.

ÖZET

ORGANOFİLİK Ag NANOTANECİKLERİN PS/PMMA KARIŞIMLARI İÇERİSİNDEKİ SEÇİMLİ YÜKLENMESİ

Nanotaneciklerin polimer karışımlarıyla birleşimi tek tür homopolimerlerle hazırlanan polimer kompozitlerin avantajlarının ötesinde malzemeye önemli özellikler sunar. Çeşitli iç yapılar içinde bileşen polimerlerin uyumsuzluğu nedeniyle bu karışımlar faz ayırımı gösterdikleri için tanecikler, fazlardan birinde bulunabilirler. Taneciklerin farklı yerleşimleri yeni mikro yapıların gelişimine; bu nedenle de fiziksel özellikleri üzerindeki kontrolüne izin verir. Bu çalışmada, Ag nanotanecikler, $AgNO_3$'ın indirgenmesiyle hazırlandı. Bu taneciklerin yüzeyi hexadecyltrimethylammonium bromide (CTAB) ile kaplandı ve tetra hidro furan (THF) içinde eşit kütleli polistiren (PS) ve polimetil metakrilat (PMMA) ile karıştırıldı. Karışım solüsyonunun katı içeriği %2.5 w/v. Taneciklerin polimer karışımlarına oranla konsantrasyonu % 0,7. Kompozit film cam yüzeye dökülerek hazırlandı. Kompozit filmlerin yüzey özellikleri atomik kuvvet mikroskopu (AFM) ve taramalı elektron mikroskopuyla (SEM) incelendi. Tanecik içermeyen kompozit filmlerin yüzeyi PMMA açısında zengin ve PS fazlar 4,5 μm çapında yuvarlak çukurlar şeklinde olduğu gözlemlendi. Tanecik boyutu küçük olduğunda (yaklaşık 20 nm), tanecikler tercihen fazların arayüzeylerine yerleştiler. 90 nm çapında daha büyük parçacıklar ise PMMA fazının içinde bulundular. Nanokompozit filmleri 165 ˚C de 3 gün tavlandıktan sonra, tanecikler boyuttan bağımsız PS fazına taşındılar ve sadece PS yönelimli kompozitler elde edildi.

TABLE OF CONTENTS

LIST OF FIGURES

Figure **Page**

LIST OF TABLES

Table **Page**

CHAPTER 1

INTRODUCTION

Polymer nanocomposites are produced by the combination of at least two dissimilar materials such that one of them has nanoscopic dimensions. They attract significant attention due to their flexibility in fabrication of novel materials with novel physical properties such as higher conductivity, better mechanical and scratch properties, better absorption/emission properties (Demir & Wegner, 2012).

The distribution of inorganic nanoparticles in polymer matrix determines the final properties of composites. Homogenous particle distribution is required for maximum performance.

When nanosized particles are dispersed into a homopolymer, the particles are randomly dispersed into the matrix volume. When polymer matrix is a block copolymer or a polymer blend where a phase separation takes place, the particles have choice to be present in any of the polymer phases. Since the fabrication of block copolymer is demanding in large scale, the employment of a polymer blend can be readily used to obtain different polymer phases and selective loading of the particles into the polymer volume. In other words, the blends to meet market requirements; they are seen faster and cheaper way rather than new polymer synthesis, and they offer the possibility to increase the mechanical properties of the material, fracture and chemical resistance, thermal properties. In this study, we employed two immiscible polymers. One of them is polystyrene (PS), which is an amorphous polymer with high thermal and radiation resistance. The other one is poly (methyl methacrylate) (PMMA) that has high transparency, high chemical and corrosion resistance to abrasion, light transmittance and insulation. By blending these two polymers, superior physical properties can be obtained.

Phase separation of polymer blends depends on following physical effects:

- **Molecular weight of polymers** longer chains are less mobile and metastable structure may be more important during annealing.
- **Composition Ratio**: The majority component has a tendency to form a continuous matrix phase.
- **Substrate Surface Energy:** PS prefers hydrophobic substrate such as H-terminated Si, While PMMA prefers hydrophilic substrates such as the Si-O and Si-OH terminated native oxide layer of a Si wafer (denoted SiO_x). When PS/PMMA thin films are casted on a Si wafer with a native oxide surface, expected that the PMMA tends to segregate to the substrate.
- **Choice of Solvent:** This affects the evaporation characteristics and inhomogenity of components in spun-cast polymer blend films
- **Annealing Procedure:** Temperatures above the glass transition temperature (~110 ˚C for PS and PMMA) are required for the polymer chains to become mobile. Increasing M_w of polymers, annealing time is also increased to approach equilibrium.(Morin et al., 2001)

Due to the larger interfacial energy with respect to surface energy difference between them, two materials will have a strong tendency to extend phase segregation right to the surface. The bulk and surface immiscibility are crucial in nanoscale pattering. This material combination is important for industrial applications. For instance, while PS-*b*-PMMA diblock copolymers are used in fabrication of high density magnetic storage media, phase separated PS/PMMA blends have been proposed as antireflection coatings.

Metallic nanoparticles show size and shape-dependent properties that are of interest for applications ranging from catalyst and sensing to optics, antibacterial activity and data storage(De Gryse et al., 2008). Silver nanoparticles have received considerable attention in their different physical, chemical and physicochemical characteristics such as increased optical, electromagnetic and catalytic properties from the bulk materials (Choi et al., 2008).

In this work, we performed a proof of concept study for the selective loading of as prepared Ag particles into the polymer blends

1.1. **Phase Separation of Polymer Blends**

Polymer blends exhibit phase separation due to the repulsive interaction between the components such as the chemical incompatibility between the polymers. The most relevant theory for representing the free energy of binary polymer mixtures is the Flory Huggins Theory.

$$w_{AB} = \frac{1}{2}\,(\varepsilon_{AA} + \varepsilon_{BB}) - \varepsilon_{AB} \qquad \text{and} \quad \chi_{AB} = \frac{z w_{AB}}{kT}$$

where ε_{ij} is energy of contacts between components, *i* and *j*, w_{AB} is the exchange energy of interacting segments. Flory-Huggins interaction parameter, χ_{AB} ; *z* is coordination number assumed equal to 8, *k* and *T* are Boltzmann constant and temperature respectively.

The basic relationship governing mixtures of polymers;

$$\Delta G_{mix} = \Delta H_{mix} - T\Delta S_{mix}$$

where ΔG_{mix} is the free energy of mixing, ΔH_{mix} is the enthalpy of mixing (heat of mixing) and ΔS_{mix} is the entropy of mixing. When ΔG_{mix} is greater than 0, phase separation occurs.

The determination of the entropy of mixing begins with the Boltzmann relationship:

$$\Delta S_{mix} = k\, ln\Omega$$

$$\Omega = \frac{N!}{N_A! - N_B!}$$

where the N_0 is number of atoms,

$$\Delta S_{mix} = k\,[ln\ N_0! - (ln\ N_A! + ln\ N_B!)]$$

Using Stirling's approximation

$$\Delta S_{mix} = k\,[(N_0 ln\ N_0 - N_0) - N_A ln\ N_A - N_B ln\ N_B)]$$

Recognizing that $N_0 = N_A + N_B$;

$$\Delta S_{mix} = k\,[(N_A + NB)\ ln\ N_0 - N_A\ ln\ N_A - N_B\ ln\ N_B$$

$$= k\,[-N_A\,(ln\ N_A - ln\ N_0) - N_B\,(ln\ N_B - ln\ N_0)]$$

$$= - k \, [N_A \, ln \, \frac{N_A}{N_0} + N_B \, ln \, \frac{N_B}{N_0} \,]$$

$$\Delta S_{mix} = - k \, N_0 \, (\frac{\phi_A}{v_A} \ell n \phi_A + \frac{\phi_B}{v_B} \ell n \phi_B)$$

where $\emptyset$ and v are volume fraction and molecular volume of segments of polymers respectively.

$$\Delta \, S_{mix} = - R \, (\frac{\phi_A}{v_A} \ell n \phi_A + \frac{\phi_B}{v_B} \ell n \phi_B)$$

$$\Delta H_{mix} = RT \chi_{AB} \phi_A \phi_B$$

$$\Delta G_{mix} = RT \, (\frac{\phi_A}{v_A} \ell n \phi_A + \frac{\phi_B}{v_B} \ell n \phi_B + \chi_{AB} \phi_A \phi_B \,)$$

For polymers, the miscibility can only be achieved when $\chi < \chi_{cr}$. The χ parameter at the critical point χ_{cr} can be obtained from the phase diagrams.

$$\chi_{cr} = \frac{1}{2} \, (\frac{1}{\sqrt{r_1}} + \frac{1}{\sqrt{r_2}})$$

where r_i is the number of polymer segments (which is proportional to the degree of polymerization).

For instance, PE/EVA blends under investigations in this work are blends of a homopolymer and a copolymer (PE/E_xVA_{1-x}). The effective interaction parameter χ between the homopolymer and the copolymer is given by:

$$\chi = x\chi_{EE} + (1-x) \, \chi_{EV} - x(1-x) \, \chi_{EV}$$

where χ_{ij} are the segmental interaction parameters and x is the copolymer composition in mol.-%. $\chi_{EE} = 0$ in the case of PE/EVA blends and therefore the effective interaction parameter χ is equal to:

$$\chi = (1-x) \, \chi_{EV} - x(1-x) \, \chi_{EV}$$

And as already mentioned, the polymers are miscible when $\chi < \chi cr$.

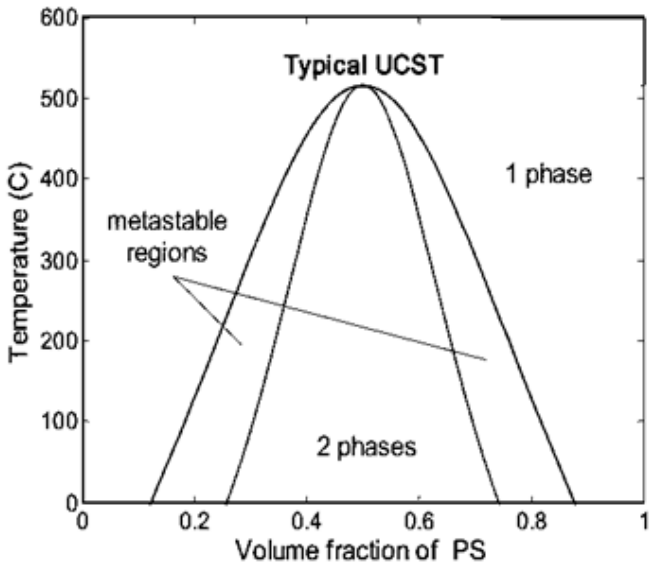

Figure 1.1. Phase Diagram of PS/PMMA polymer blend.
(Source: Ha, Atallah, & Krishnamoorti, 2011)

A schematic phase diagram of PS and PMMA is shown in Figure 1.1, phase separation occurs from 0 ˚C to 500 ˚C when volume fraction PS is 0.5. That is why the volume fraction was 0.5 through our study.

In the following is enthalpic interaction between nanoparticles and polymers in blends. Ginzburg et al. (He, Ginzburg,& Balazs, 2006) assumed that a particle interacts with both polymers A and B. ($\chi_{AP}>0$ and $\chi_{BP}>0$) and introduced the variables $x= \phi \chi_{AP} + (1-\phi) \chi_{BP}$ and $y= (\chi_{AP} - \chi_{BP})/2$, where ϕ and $(1-\phi)$ volume fraction of polymers and χ is Flory and Huggins interaction parameter.

The variable *x* was explained that is a measure of the average enthalpic 'field' acting on the particles, due to the homopolymers and *y* is a measure of the relative affinity between the particles and the different homopolymers; when *y* is negative, the particles prefer the A phase, while a positive *y* indicates a preferential interaction between the particles and the B phase.(He, Ginzburg, & Balazs, 2006)

For another estimation in order to explain the location of nanoparticle consideration is Young's equation by calculation of the wetting coefficient ω_a ;

$$\omega_a = \frac{\gamma_{P1} - \gamma_{P2}}{\gamma_{12}}$$

where γ_{P1} and γ_{P2} are interfacial tension between polymer 1 and the nanoparticles, polymer 2 and the nanoparticles respectively. γ_{12} prefers to interfacial tension between the polymers. If the wetting coefficient is higher than 1, the nanoparticles are located in the Polymer 1, when having values lower than -1 they are located in polymer 2, and if the wetting coefficient is between 1 and -1 the nanoparticles are preferentially located at the interface between both polymers. (Pötschke, Pegel, Claes, & Bonduel, 2008)

Ginzburg and co-workers (He, Ginzburg, & Balazs, 2006) examined that when χ_{AB} is greater than both χ_{AP} and χ_{BP}, the particles can act as compatibilizers, causing the entire system to be miscible. For instance; studied on styrene-acrylonitrile(SAN)/ethylene-propylene diene monomer rubber(EPDM) are immiscible blend. It was found that the addition of surface treated calcium carbonate fillers allowed them to control the filler polymer interactions and consequently, create a miscible mixture. (He, Ginzburg, & Balazs, 2006)

1.2. **Literature Review on BCP/Nanoparticle Composite Systems**

There are few or no studies in literature for the examination of particle location in polymer nanocomposites prepared by polymer blends. However, the literature is relatively rich in terms of selective loading of nanoparticles in block copolymers. In the following, literature of BCP composites is reviewed. For example, Ton. That et al. (Ton-That, Shard, Teare, & Bradley, 2001) claimed that to reduce the interfacial tension, the coarsening of the domains near to the surface to equilibrium will take place upon annealing. Figure 1.2 is a schematic illustration of the phase behavior PS/PMMA blends upon annealing time.

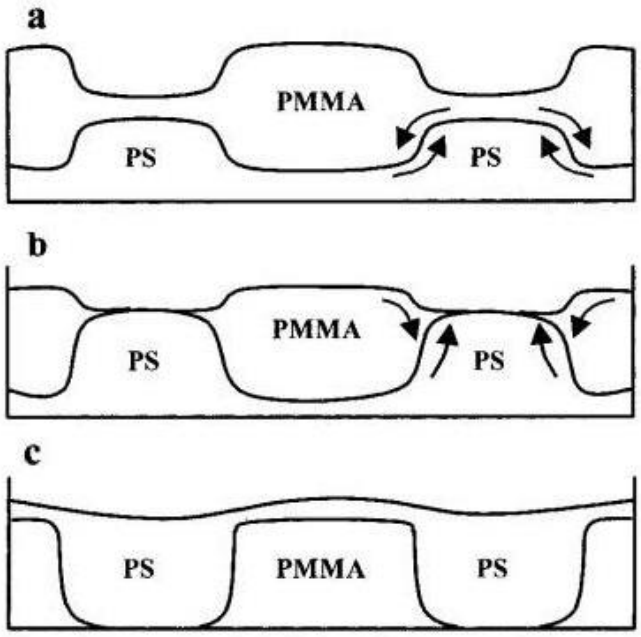

Figure 1.2. Structural model of PS/PMMA blends as spin-cast a) and upon annealing above the glass transition temperature in early stage b) and later stage c). Arrows indicate the movements of the PS-rich and PMMA-rich domains at their interface. (Source: Ton-That, Shard, Teare, & Bonduel, 2008).

In addition, they showed that different compositions and thickness of PS and PMMA films releaved different phase morphology. As shown in Fig. 1.3(a) and (f) belongs to the pure polymer films with 1% wt/v(polymer blend/chloroform). For the polymer blends containing 75%PS:25% PMMA, the AFM topography shows a pitted surface (Fig.1.3(b)). The pits have a broad, shallow structure with typical diameter ranging from 300 to 600 nm and depths of between 15 and 25 nm. A pitted surface morphology as shown in Fig. 1.3(c) was also observed for 50%PS:50%PMMA films, the pits are larger than those in the 75%PS:25%PMMA films and their diameter being between 1.2 and 1.6 μm with depths of 30±40 nm. When the polymer composition is changed to 40% PS: 60% PMMA, the surface tends to show a granular morphology (Fig. 1.3(d)). The granules have diameters of about 400 nm and protrude above the surface material by 15±30 nm. With 25% PS:75% PMMA film, the topography also shows a granular surface, but the granules are larger in size with diameters of about 1±1.3 μm. (Ton-That, Shard, Teare, & Bonduel, 2008).

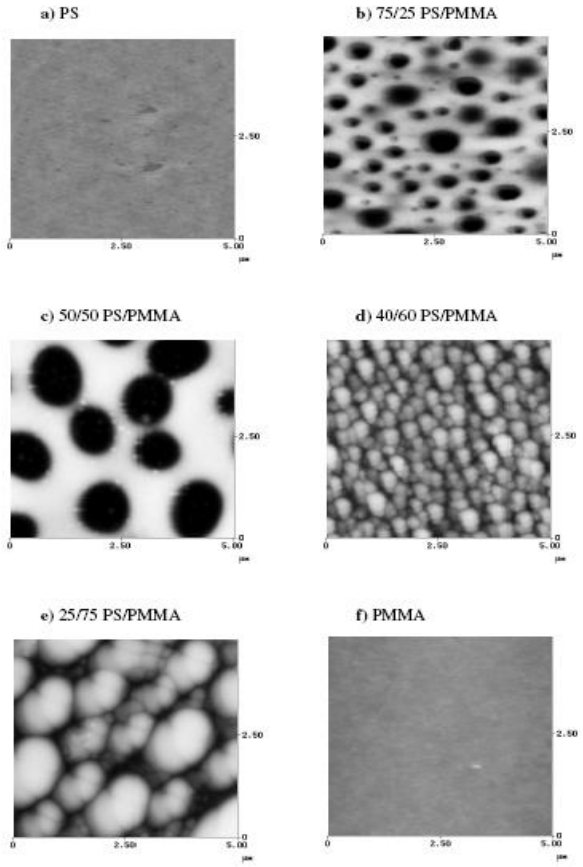

Figure 1.3. AFM images of the surface topography of PS and PMMA in single component and blended thin films cast from 1% (w/v) solution. (Source: Ton-That, Shard, Teare, & Bonduel, 2008)

Proscycevas et al. (Prosycevas, Tamulevicius, & Guobiene, 2004) investigated that solvent cast thin films of blends PS and PMMA with nominal compositions ranging from 25:75 (w/v) up to 75:25 w/v PS:PMMA with toluene as the mutual solvent on crystalline Si (100) and silica substrates. In figure 1.4 solvent cast thin films of blends PS and PMMA with nominal compositions are ranging from 25:75 wt.%:v% (w/v) up to 75:25 w/v PSyPMMA with toluene as the mutual solvent on crystalline Si (100) and silica substrates. Additionally, they proposed that morphology of the nanostructured thin film depends on the polymer concentration of the solution.(Prosycevas, Tamulevicius, & Guobiene, 2004)

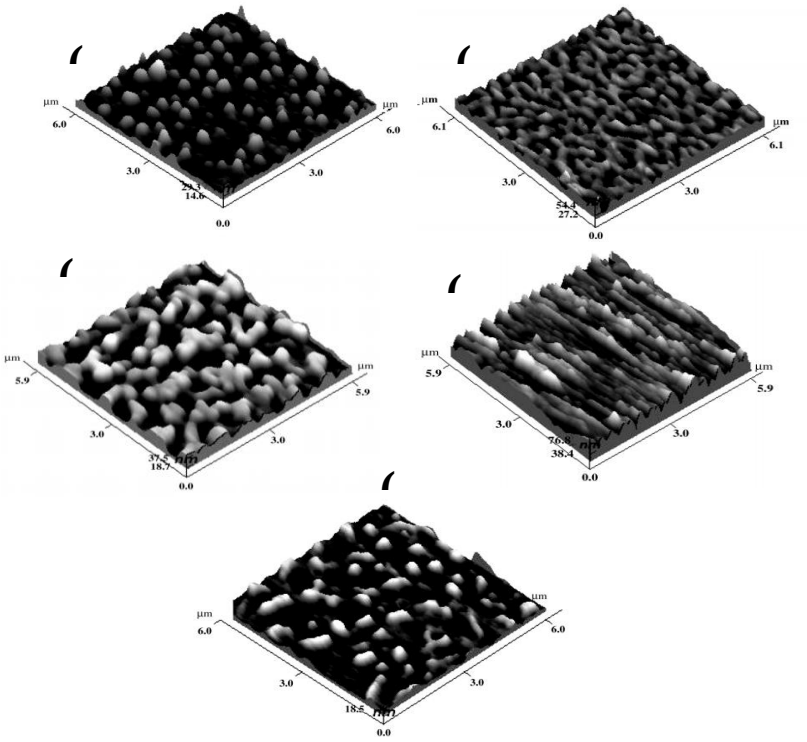

Figure 1.4. AFM images of a dip-coated a) PS film (with film thickness A=60 nm), b)PS25%:PMMA75% film (with film thickness A=40 nm), c)PS50%:PMMA50% film (film thickness A=40 nm), d) PS75%:PMMA25% film (film thickness A=80 nm) on crystalline Si(100), e) PS75%:PMMA25% film (film thickness A=20 nm) on silica.(Source: Prosycevas, Tamulevicius, & Guobiene, 2004)

Chung et al reported the examination of silica particle location in dPMMA-SAN.In figure 1.5, SEM images of polymer blends of deuterated poly(methyl methacrylate)(dPMMA):poly(styrene-ran-acrylonitrile)(SAN) thin films with 10 wt% methyl and hydroxyl coated silica, with 22 nm diameter (MST) (b, c) and 10 wt% silica with a shell of grafted PMMA brushes, with 18 nm diameter (P2K) (d, e). Initially, MST (b) and P2K (d) are homogeneously dispersed. Upon annealing at 195 □C for 24 h, MST NPs partition into the dPMMA phase (c), whereas P2K NPs segregate at the dPMMA/SAN interface (e). (Chung, Ohno, Fukuda, & Composto, 2005)

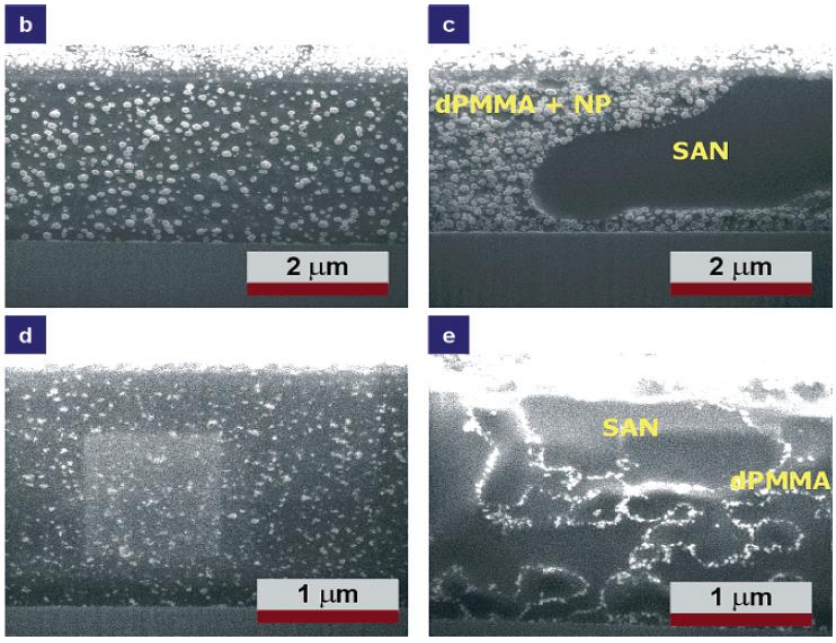

Figure 1.5. SEM images of dPMMA:SAN films with 10 wt% MST (b,c) and 10 wt% P2K (d, e). (Source: Chung, Ohno, Fukuda, & Composto, 2005)

1.2.1. Thermodynamics of Polymer/Particle Composites

Enthalpy and entropy are two main thermodynamic functions. Although they are first recognized for gaseous system, they are defined for different systems. For the particular case of our particular system based on polymers associated with particle, they are defined as follows:

Enthalpy can be roughly defined as chemical affinity between particle surface and surrounding polymer. On the other hand, *entropy* is combination of two sub functions:

i) the distortion of polymer chains in the presence of nanoparticles ii) the arrangement of the particles in polymer volume.

Research studies about selective loading of nanoparticles in polymer domains have heavily focused on the block copolymer nanocomposites with respect to polymer blend nanocomposites. Size and surface chemistry of nanoparticles have important role in determination of placement of NPs in polymer domains. Chui et al. (Chui et al., 2007) controlled the nanoparticles by mixing homopolymer blends or random

copolymers and also they claimed that the surface coverage of the polymer ligands on the nanoparticle is a critical parameter that determines the spatial organization of the nanoparticles in polymer domains. (Chiu et al., 2007)

The earliest work by Balazs' group has combined density functional theory and self-consistent field theory to simulate the behavior of nanoparticles of diameter *d* in polymer domains of period *L*. The ratio of diameter of nanoparticles *d* over domain spacing *L* controls the location of particles in the composite structure. They claimed that when the ratio of *d/L* is small, the particles are locate at the interface of the domains. However, when the ratio greater than 0.3, nanoparticles become more localized toward the center of the appropriate domains to minimize the conformational entropic penalty as chain stretching becomes significant to accommodate the nanoparticles. (Kao, Thorkelsson, Bai, Rancatore, & Xu, 2013)

Bockstaller et al. (Bockstaller, Mickiewicz, & Thomas, 2005) showed that the effect of entropy on the spatial distribution of Au and SiO_2 nanoparticles of different sizes. Experimentalists resulted the ratio of *d/L* depends on nanoparticle size, ligand size and molecular weight of polymers. While for smaller Au nanoparticles the *d/L* ratio is 0.06 which placed along the inter-material diving force, for larger SiO_2 nanoparticles the ratio is 0.26 which located the center of the domain shown in Figure 1.6. For large particles, the decrease in conformational entropy of the respective polymer chains upon particle sequestration is dominant, whereas for smaller particles, the decrease in entropy is offset by the particle's translational entropy.(Bockstaller, Mickiewicz, & Thomas, 2005)

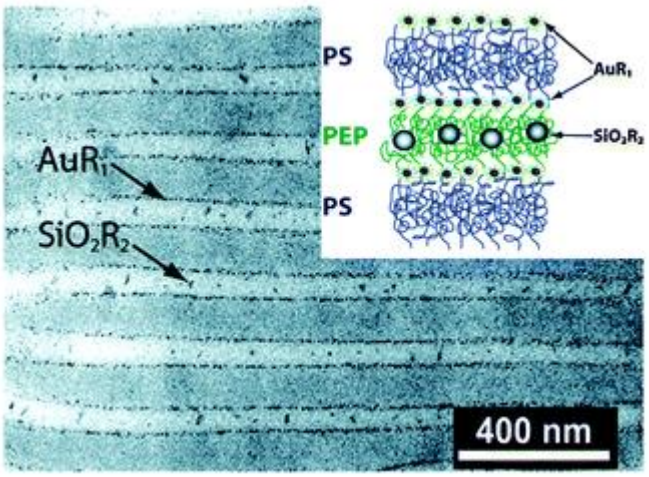

Figure 1.6. TEM micrograph of a ternary blend of PS-*b*- PEP, ~3.5 nm Au nanoparticles, and ~21.5 nm SiO_2 nanoparticles with the volume fraction of the nanoparticles around inorganic filling fraction φ = 0.02. (Source: Bockstaller, Mickiewicz, & Thomas, 2005)

CHAPTER 2

EXPERIMENTAL STUDY

2.1. Chemical and Reagents

Sodium borohydride $NaBH_4$ (Sigma-Aldrich, 99.99%) , silver nitrate $AgNO_3$ (Alfa Aesar, 99+%) , Polystyrene (PS) (Aldrich Chemical Co. , Mw ~ 350,000) , Poly(metyl methacrylate) (PMMA) (Aldrich Chemical Co. , Mw ~ 15,000) , Tetrahydrofuran (THF) (VWR International bvba/sprl), Hexadecyltrimethylammonium bromide (CTAB) (Sigma Aldrich) were used as they were without applying further purification.

2.2. Synthesis of Organophilic Silver Nanoparticles

A two-step previous was applied for the synthesis of organophilic Ag NPs. Figure 2.1 shows schematic view of the entire particle preparation Ag NPs. In the first step, naked Ag NPs were obtained via a redox reaction taking place between $NaBH_4$ and $AgNO_3$. A 10 mL of aliquiot of 0.01 M $AgNO_3$ was added dropwise (about 1 drop/second) to 30 mL of 0.02 M of $NaBH_4$ solution that had been chilled in an ice bath. The reaction mixture was stirred vigorously on a magnetic plate. (Mulfinger et al., 2007)

The redox reaction can be represented by :

$$AgNO_3(aq) + NaBH_4(aq) \longrightarrow Ag(s) + ½\ H_2(g) + ½\ B_2H_6(g) + NaNO_3(aq)$$

The dispersion mixture turned to light yellow after the addition of 2mL of $AgNO_3$ and when all of the $AgNO_3$ was added, yellow dispersion in water was obtained. The resulting particles are hydrophilic in nature.

In the second step, Ag surface functionalization was applied to make them organophilic. Hexadecyltrimethyl ammonium bromide(CTAB) was used for the surface

modification. CTAB solution was prepared in water at two different concentrations: 0.02 M and 0.002 M. CTAB solution in water was added to dispersion of silver nanoparticles as 1/20 ratio (1 mL CTAB for 40 mL of silver nanoparticle dispersion). After addition of CTAB, the solution has been sonicated until CTAB was dissolved in solution. Then, the final solution was centrifuged at 6000 rpm for 40 min.

The Ag/CTAB nanoparticles were isolated. After decanting the water solution, the precipitation was dried and powder Ag/CTAB nanoparticles was obtained.

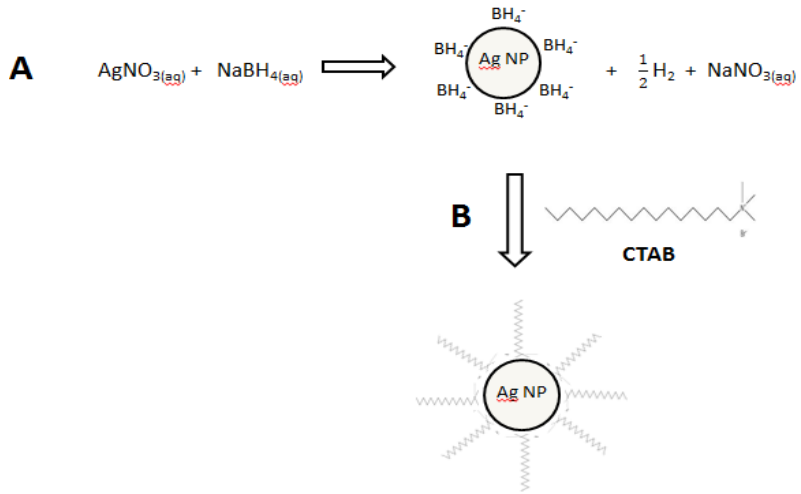

Figure 2.1. Schematic representation of reaction A) Synthesis of Ag Nanoparticles and B) Coating surface of Ag NPs with CTAB.

2.3. **Preparation of Ag/PS-PMMA Blends of The Composite Films**

Polymer blend solutions were prepared by dissolving of PS and PMMA as 1:1 weight ratio in THF as 2.5% (w/v). After complete dissolution of the polymers, the powder of Ag/CTAB nanoparticles was added into the polymer solution mixture.

Polymer nanocomposites films were prepared by casting the dispersion mixture on glass surface using micropipette. Schematic illustration of the preparation of cast film method is given in Figure 2.2. The films were cooled at 25 ˚C and annealed at 165 ˚C.

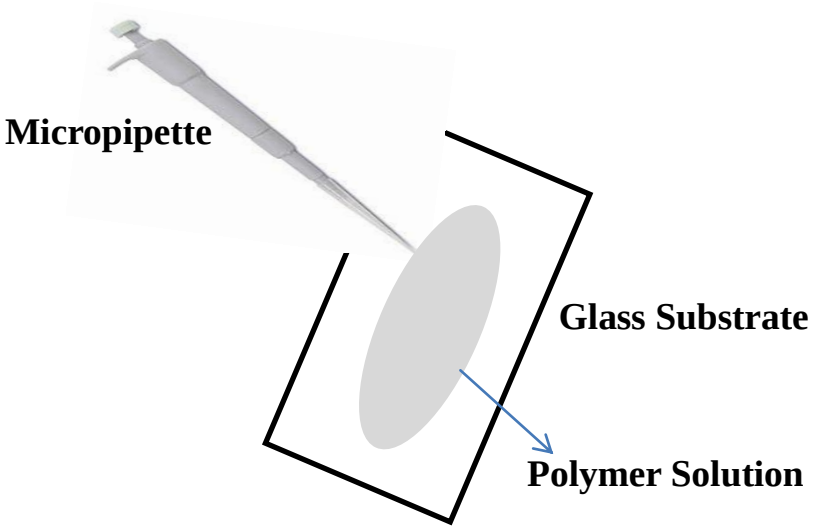

Figure 2.2. Schematic representation of cast film process

2.4. **Characterization of Samples**

Characterization of Ag and Ag/CTAB nanoparticles and their composites with PS/PMMA thin polymer nanocomposite films were performed using the techniques given below.

Scanning Electron Microscopy (SEM) is used to investigate the surface morphology of the polymer nanocomposites. In our study, Phillips XL-30S FEG and ESEM Quanta 250 FEG were used to observe the morphology of the surfaces. Sample surfaces are scanned with the electron beam and resulting image formed by secondary electrons is determined. Therefore, this method provides information about the surface chemistry and topography by the surface reflection. (Goldstein et. al.2003)

For Atomic Force Microscopy (AFM), Multi Mode SPM Nanoscope IV was used to investigate the phase separation and location of NPs on the surface of the samples. AFM images are obtained by measurement of the force on a sharp tip created by the proximity to the surface of the sample. This force is kept small and at a constant level with a feedback mechanism. When the tip is moved sideways it will follow the surface contours.

Dynamic Light Scattering (DLS) is the most convenient method for measurement of particle size in dispersion. Shining a monochromatic light beam, such

as a laser, onto a solution with spherical particles in Brownian motion causes a Doppler Shift when the light hits the moving particle, changing the wavelength of the incoming light. This change is related to the size of the particle. The surface charge is determined by applying potential and measured the potential difference of the dispersion of the particles. (Sartor 2003). Malvern Zeta Size was used to measure of size distribution and surface charge of the nanoparticles and obtained data are plotted by using Origin Pro8.

Uv-Vis Spectrometer is based on absorption of photons that it is excited to upper energy level, then returns back to its ground state and so energy appears in process. Schimadzu UV 2550 was performed to measure absorbance of light of the samples and the worked wavelength range was 200-700 nm.

Thermal Gravimetric Analysis (TGA) was used to examine grafting density of surfactant and polymer, moisture and nanoparticle of polymer nanocomposites. TGA analysis was applied from 0 ˚C to 600 ˚C with O_2 gas. Perkin Elmer Diomand TG/DTA was used and result data was plotted by Origin Pro8.

Differential Scattering Calorimetry, DSC Q10 V9.4 Build 287 was used to measure glass transition temperature of the thin film samples. DSC analysis was applied from 25 ˚C to 160 ˚C under N2 gas with 50.0 ml/min of flow rate and aluminum pan.

Nuclear Magnetic Resonance (NMR) Spectroscopy, NMR Varian 400 Mhz was used to identify surfactant molecule on the surface of the nanoparticles. Deuterated Dimethyl sulfoxide (DMSO) was used as the solvent.

CHAPTER 3

RESULTS AND DISCUSSION

2.5. Synthesis of Ag Nanoparticles

Ag nanoparticles were synthesized by reduction of $AgNO_3$ via $NaBH_4$ in aqueous solution. The resulting dispersion is yellow. It is a quite stable dispersion. Sedimentation of the particles was not observed for more than one month. The concentration of starting material $AgNO_3$ was 0.01 M. When the concentration increases, the color of dispersion is turned out to be dark. The change in color is most probably due to the aggregation of individual particles. The reaction mixture was cast on a cupper grid and after solvent evaporation; the surface of the grid is scanned by Transmission Electron Microscopy (TEM). Figure 3.1 presents an overview and higher resolution images of the particles. The particles appear spherical with a diameter of 6 nm on average and separate as islands. They are most probably capped by BH_4 (-) ions and electrostatically stabilized such that the particles are no aggregated. The inset of right panel shows electron diffraction pattern of the particles. There are discrete sharp circles indicating that the particles have high crystallinity.

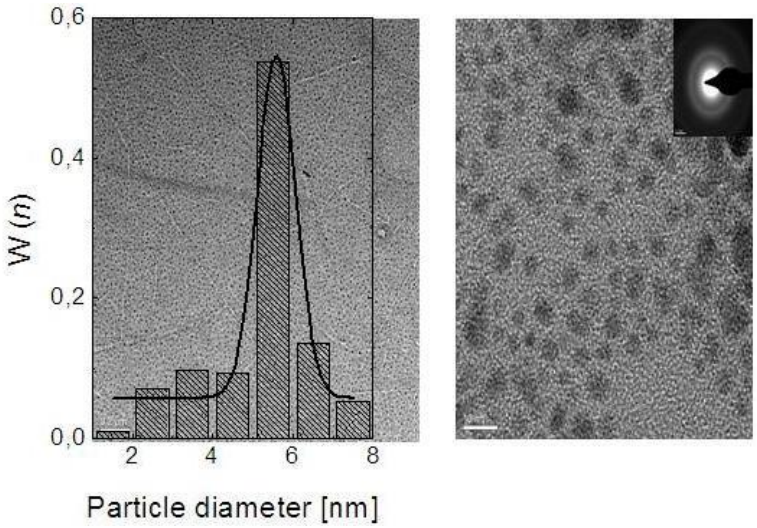

Figure 3.1. TEM image of Ag nanoparticles

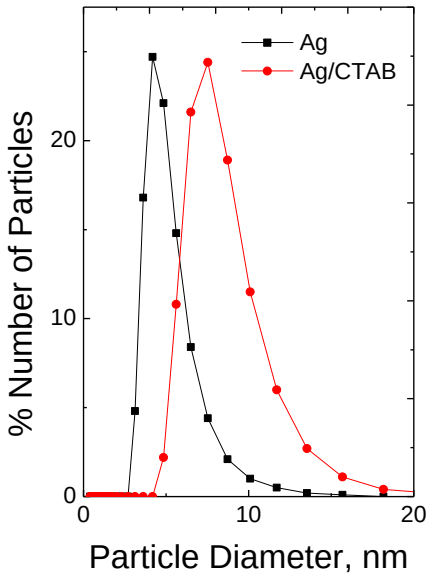

Figure 3.2. DLS number Size distribution of Ag and CTAB capped Ag particles.

Figure 3.2. illustrates DLS number size distribution of the both naked and CTAB capped particles. The mean diameter of naked Ag particles have 6 nm in diameter. This result compatible with the particle size obtained from TEM. When the particles are modified by CTAB the size increase to 9 nm. The length of the surfactant molecule

contributed for the increase of the diameter. The length of the molecule is around 1.5 nm on average.

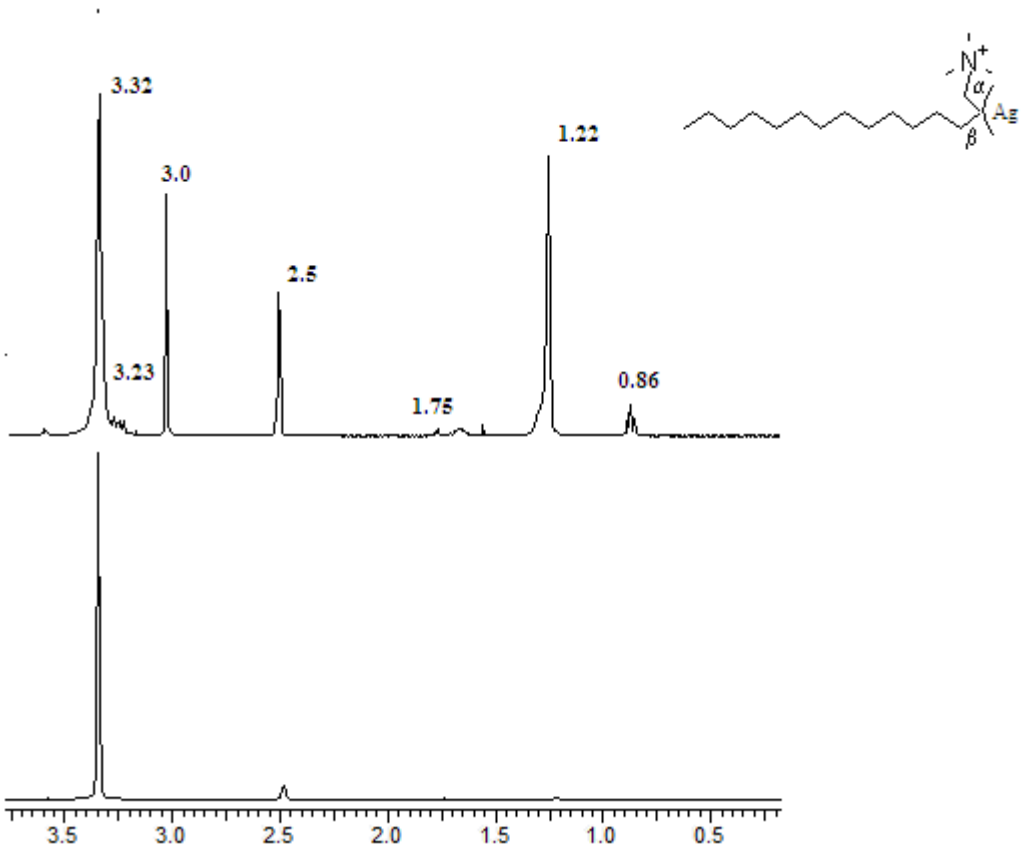

Figure 3.3. NMR spectra for Ag/CTAB NPs with different carbon atom.

CTAB molecules on the surface of the Ag NPs were identified by using NMR spectroscopy and chemical shifts are presented in Figure 3.3. The signals of α-CH_2 appears at chemical shift δ = 3.39 ppm for neat CTAB and at 3.23 ppm in Figure 3.3 for Ag/CTAB. Its multiplet appearance had been attributed to H-H coupling to β-CH_2. Due to methyl protons of CTAB polar groups, there are narrow signals at 3.0 ppm, this value is at 3.16 ppm for pure CTAB. The broad humps at 1.80 ppm for pure CTAB and at 1.75 for Ag/CTAB NPs are β-CH_2. The peaks at 1.22 ppm and 0.86 ppm are combined resonances of the other methylenes in the alkyl chains referred as main chain peaks. The signals at 3.32 ppm and 2.5 ppm are d-DMSO (solvent) and H_2O respectively. Sui et al. (Sui et al., 2006) compared the neat CTAB and Ag NPs and suggested that the larger changes of the protons on α-CH_2 and β-CH_2 than that on N-CH_3, however, indicate that the capping of CTAB molecules on Ag NPs is through their head groups with Ag NPs located between β-CH_2 and nitrogen atom. (Sui et al., 2006)

The pictures of Ag and Ag/CTAB dispersions and absorbance of light are shown in Figure 3.4. Yellow dispersion refers to Ag NPs and the black one is for Ag/CTAB NPs. The spectra of the particles show the difference between the particles before and after capped with CTAB. Naked particles have sharp signal centered at 400 nm. Upon capping the particles with CTAB, the main signal remains unchanged; however, a shoulder around 450 nm appears. This new signal can be attributed to the presence of agglomerated Ag/CTAB particles. In addition, the colour of particle dispersion changes from yellow to black. Since agglomeration is observed in spectroscopy, steric stabilization of the particles by CTAB is not as much effective as electrostatic stabilization of the naked particle.

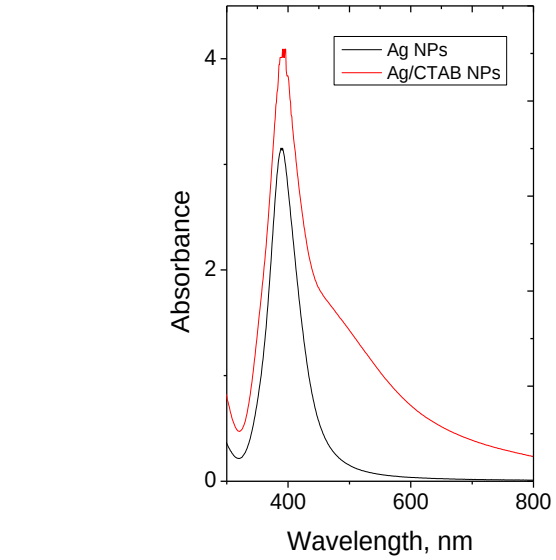

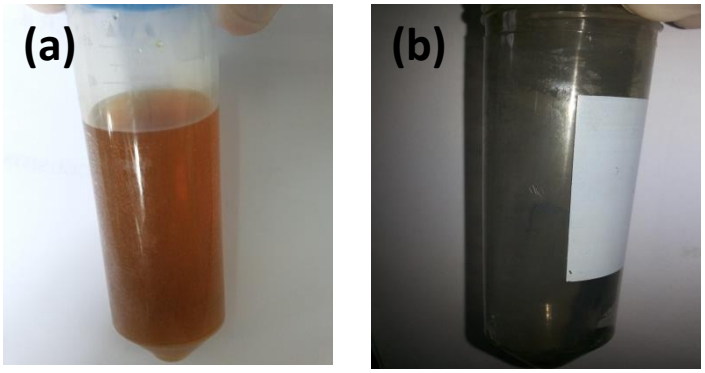

Figure 3.4. Absorbance spectrum of before functionalization with CTAB and after CTAB treatment. a) Ag nanoparticles dispersion in water, b) Ag/CTAB NPs.

The surface charge of the Ag and Ag/CTAB NPs were analyzed by the zeta sizer as a proof of the surface modification. In Figure 3.5 shows zeta potential of the Ag NPs before and after capped with CTAB. The surface charge of naked Ag particles is around -47 mV. We postulated that the surface of Ag nanoparticles is covered by BH4- ions. The particles repel each other so that the dispersion is electrostatically stabilized. After the capping process with CTAB as the cationic surfactant, the surface charge of particle was found to be +34mV. The absolute value of surface potentials is similar in terms of absolute value. One can speculate that the majority of the negative center on the particles surface is capped by quaternary ammonium salt molecules.

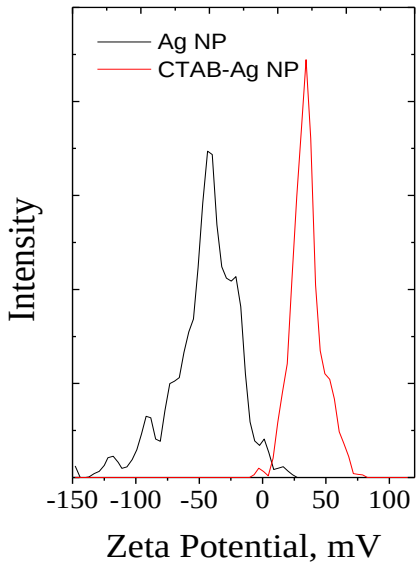

Figure 3.5. Surface potential values; black line: before functionalization with redline: after CTAB treatment.

Figure 3.6 shows the zeta potential of CTAB capped Ag nanoparticles while increasing the amount of CTAB solution treated with a known amount of reaction mixture. In these experiments, we employed 2.5% volume of CTAB solution with Ag nanoparticle dispersion. For testing, we employed higher volume of CTAB solution. The result shows that increasing volume of solution does not change the potential of Ag particles. In another words, there is no more negative BH_4(-) centers to be occupied by CTAB molecules.

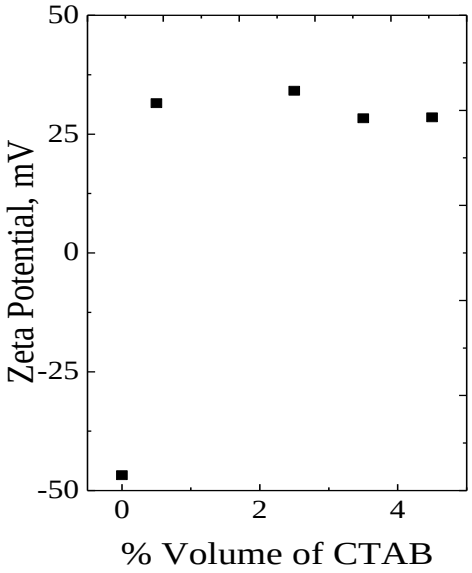

Figure 3.6. Surface potential values by adding different volume of CTAB solution.

Colloidal Ag nanoparticles were isolated by centrifugation. The nanoparticles were analyzed in powder form. Figure 3.7 presents SEM images of the Ag powder on metallic stub. Since the particles are in dry state, imaging of the single particle cannot be resolved, rather an agglomeration of the single nanoparticles. In addition, the Ag nanoparticles are agglomerated when they are not synthesized in ice bath or storage in refrigerator after synthesized.

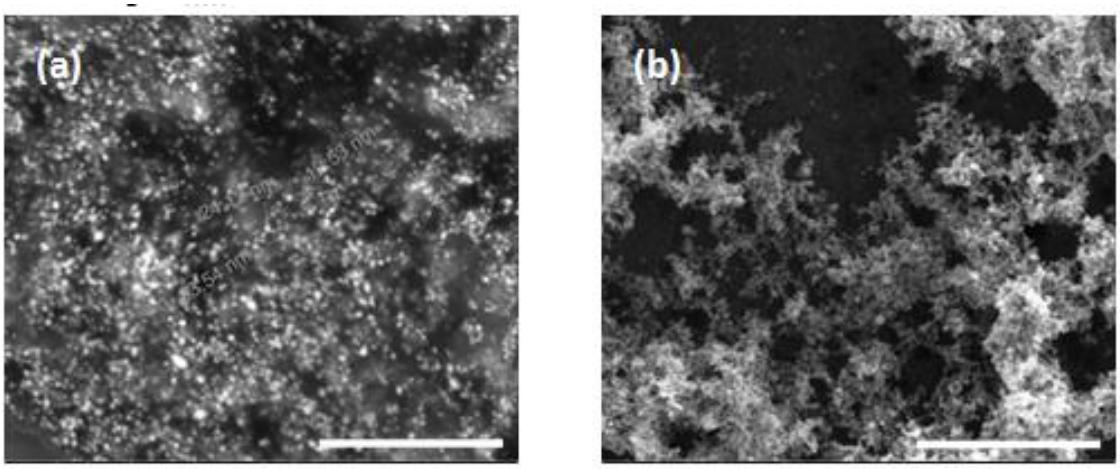

Figure 3.7. a) SEM Image of Ag nanoparticles, 1μm b) SEM images of agglomerated Ag nanoparticles, 1μm.

The surface capped particles were imaged by STEM detector. The representative result is given in Figure 3.8. It shows STEM image of the nanoparticles before and after modification. Before the modification, the NPs seem individual and after the process, they located as large particle domain. The images show that surface capping process does not cause a remarkable difference in morphology of the nanoparticles in terms of shape and size.

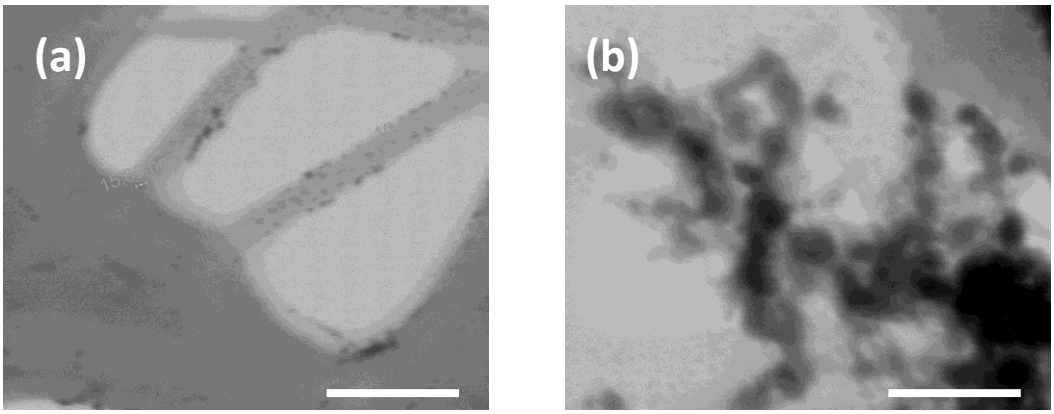

Figure 3.8. a) STEM Image of Ag nanoparticles b) STEM images of Ag/CTAB nanoparticles. The scale bars refer to 200 nm.

Surface capping of the nanoparticles was carried out by two different concentrations of CTAB solution: 0.02 M and 2.0 mM. Atomic weight percentage of

Nitrogen on Ag NPs was measured by EDX. The results are given in Fig. 3.9. While the weight percentage of N is 4.22% in Ag NPs capped with 2.0 mM CTAB, the percentage increases to 6.95% in Ag NPS capped with 0.02 M of CTAB. Not surprisingly, increasing concentration of CTAB increases the nitrogen content on the particle surface.

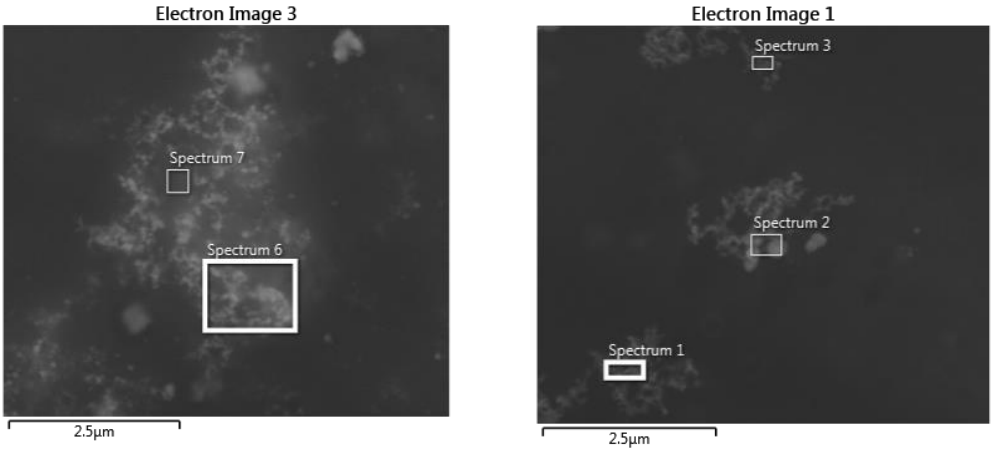

Spectrum 6			Spectrum 1	
Element	**2 mM CTAB**		**0.02 M CTAB**	
	Wt%	Atomic %	Wt%	Atomic %
C	3.47	5.15	7.10	12.58
N	4.22	5.37	6.95	10.56
O	78.24	87.16	52.88	70.34
Ag	14.07	2.32	33.07	6.52
Total:	100.00	100.00	100.00	100.00

Figure 3.9. EDX result of Spectrum 6) 2 mM of CTAB capped Ag nanoparticles b) 0.02 M of CTAB capped with Ag Nanoparticles.

The particles are capped with CTAB molecules such that inorganic core is covered by organic molecules. The amount of organic residue covering the core can be understood via thermogravimety.

Table 3.1 is produced based on the TGA measurements of Ag/CTAB NPs and literature values based on decomposition temperature range of pure CTAB between 207-316 ˚C. The thermogravimetry results are agree with literature. The particles were analyzed room temperature to 650 ˚C.

Table 3.1. The weight loss processes of pure CTAB and the Ag/CTAB NPs sample with their assignments in TGA experiment.

	Weight Loss Range (°C)	**Weight Loss (%)**
Pure CTAB*	207-316	100
The Ag/CTAB NPs	100-120	4.12
	120-468	8.35
	468-600	0.45

***(Sui et al., 2006)*

The thermogram is given in Figure 3.10. There are two important weight loss values, fist one is between 100-120 ˚C which caused by moisture or solvent residuals. The other is between 120-468 ˚C decomposition of CTAB molecules. There is no remarkable mass remained after 468 ˚C , one can claim that metallic Ag particles are capped by organic CTAB percentage weight of CTAB molecule on the surface of Ag is 8.35%.

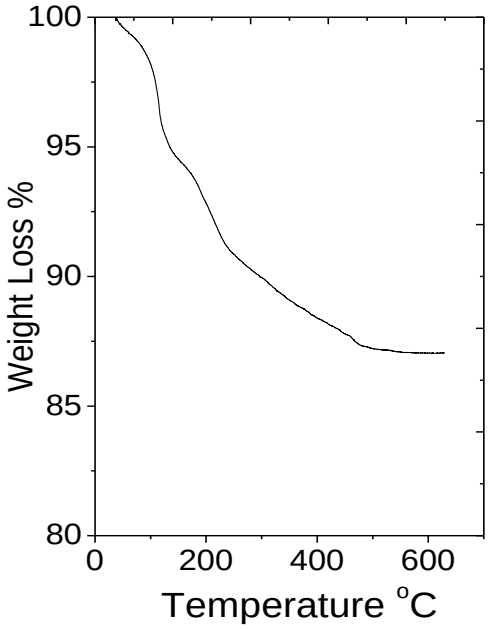

Figure 3.10. TGA results of Ag/CTAB NPs

2.6. **PMMA/PS Blends**

Figure 3.11 presents tapping mode AFM images of the PS (left panel) and PS:PMMA blend prepared 1:1 ratio (right panel) by mass. Both polymeric components are immiscible and undergo phase separation. The blend shows pitted surface morphology. The pits seem spherical in shape and homogeneously dispersed throughout the film surface. The dark pits refer to PS and light regions are PMMA. The size of the pits is around 4.5 μm. This size is larger compared to the size of PS in literature. The size reported in literature depends on the molecular weight of polymers employed. Since molecular weight of PS is much heavier than PMMA, the size of the pits can be larger compared to literature. One can expect that the surface should be covered with lower surface energy PS molecules. However, PMMA is also present on the surface of the film. The reason could be the better solubility of PMMA in solvent compared to PS.

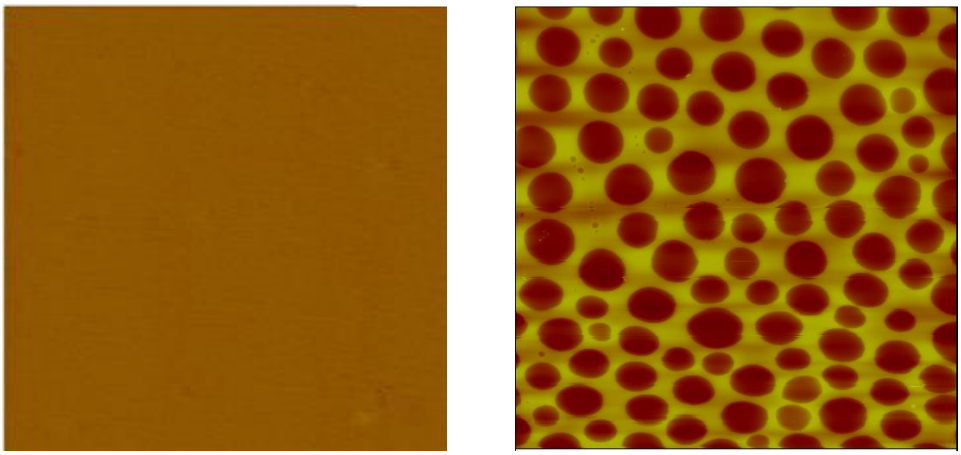

Figure 3.11. Tapping mode AFM images of PS(5x5 μm) and PS:PMMA(50x50μm) blends at 25 ˚C.

Table 3.2 is calculated the data in literature about the surface tension of polymer domains and surfactant on the surface of the Ag NPs at 25 ˚C and 165 ˚C by using linear interpolation of literature data. While At 25˚C, the surface tension of CTAB is closer to PMMA, at 165 ˚C this value is closer to PS phase.

Table 3.2. Surface tension of polymers and the surfactant at different temperature.

Temperature, ˚C	Surface Tension,mN/m		
	CTAB[a]	PS[b]	PMMA[c]
25	40.03	39.0	41.0
165	35.6	31.6	30.1

a;(Tang, Du,Yang, & Zhang, 2006), b and c; (Wu,1970)

2.7. Nanocomposites prepared by PS-PMMA blend and Ag nanoparticles

In polymer/nanoparticle composites, glass transition temperature (T_g) hint about the interaction of particle surface and surrounding polymer chains. Figure 3.12 presents the thermogram of the polymer blend, polymer composite prepared by blend, and polymer composite annealed at 165 ˚C. T_g values of PS and PMMA are 105 ˚C and 104 ˚C in the literature. For the blends prepared in this thesis, a single appears. We can claim that the values were measured close to each other and the signals overlap. The incorporation of the Ag/CTAB particle into system, T_g value remains unchanged. This result indicates that Ag particles are inert to both polymeric components and there is no specific affinity between the particle surface and PS and PMMA chains.

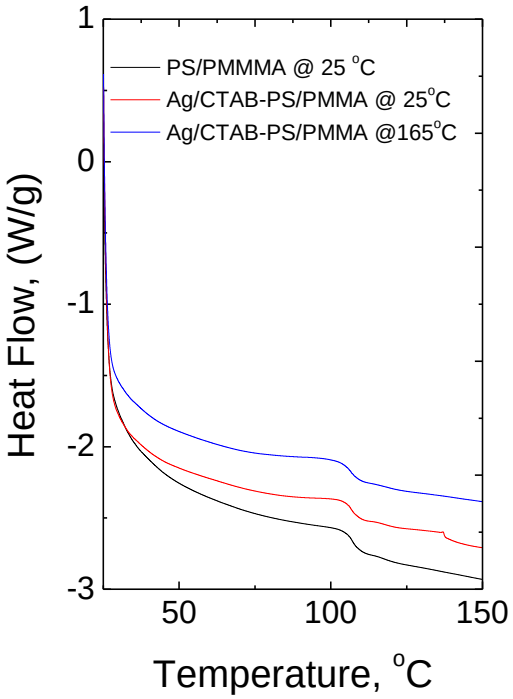

Figure 3.12. Glass transition temperature of polymer nanocomposite films.

Figure 3.13 presents tapping mode AFM images of the composites. The bright regions refer to Ag, and the large spherical regions refer to PS and the rest darker regions are PMMA. It is shown that the particles are merely located at PMMA phase. The size of particle domains is nearly 90 nm. The particles used in this sample were prepared by reduction of $AgNO_3$(aq). When the concentration of CTAB was increased, the grafting density of CTAB is higher. The higher the density, the better stability and smaller particle domains. As a result, the size of Ag particle domains is reduced to 20 nm. The location of particles is strongly depends on the size. When the size is small, the particles are sequestered at the interface of PS and PMMA domains. (Fig. 3.14-3.15) Theoretical studies support our results. Thompson et al. suggested that *d/L* ratio governs the location of the particles (Thompson, Ginzburg, Matsen, & Balazs, 2001).

The ratio of diameter of nanoparticles *d* over domain spacing *L* governs the location of particles in the composite structure. Theoretical studies suggest that smaller particles with a ratio (*d*/*L*) is located at interface of the domains. Based on the AFM images, the average size of the NPs located in PMMA (a and b in Figure 3.13) is approximately 90 nm.

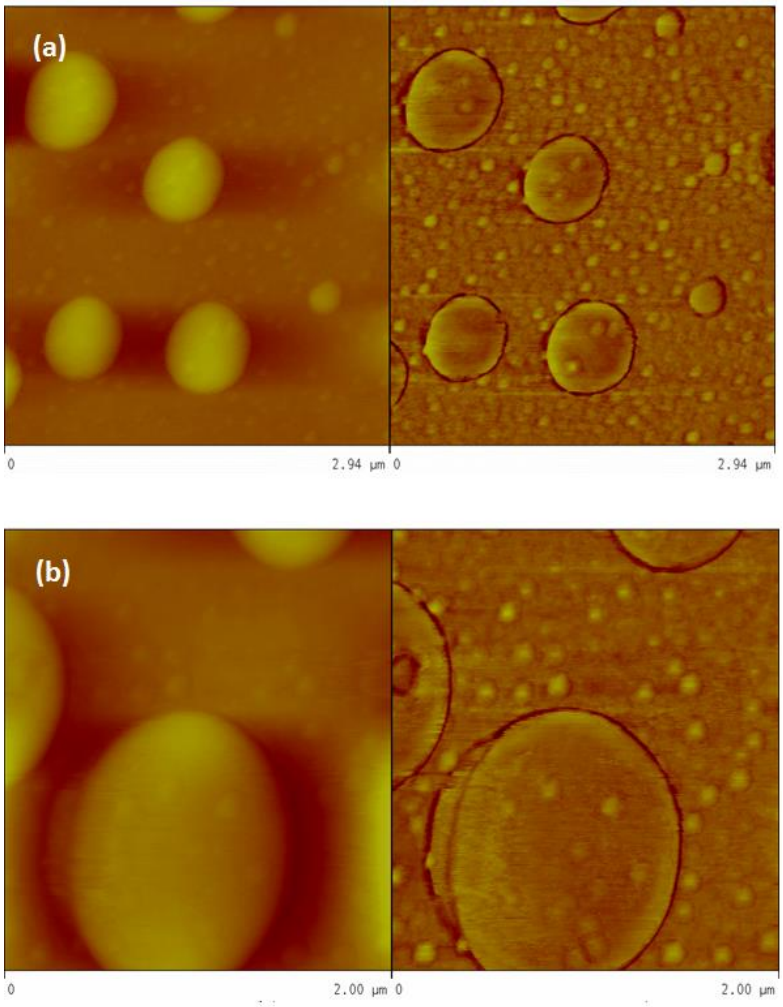

Figure 3.13. Tapping mode AFM images of AG/CTAB-PS/ PMMA nanocomposite films at 25 ˚C, the particles in a) and b) in PMMA domain.

Additionally, in Figure 3.13, the ratio of particle diameter to PS phase diameter (*d/L*) is 0.15. For Figure 3.14 a and b, this ratio is 0.093. As the nanoparticle diameter (27 nm) and *d/L* is decreased, the NPs are located at the interface.

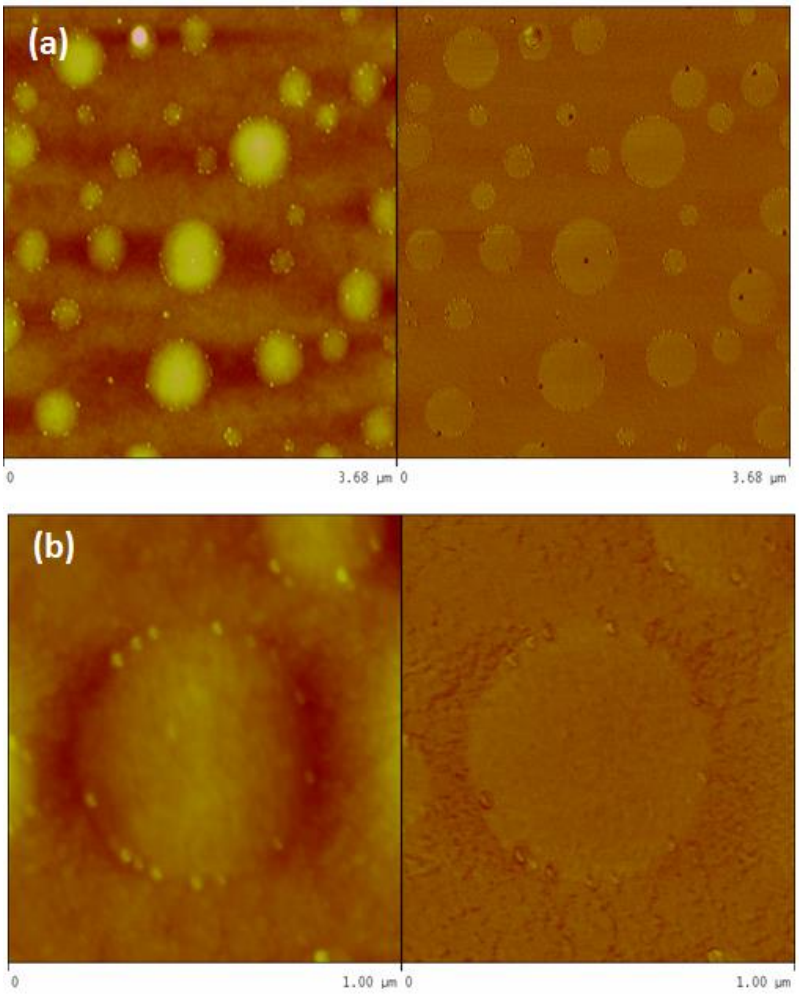

Figure 3.14. Tapping mode AFM images of Ag/CTAB-PS/ PMMA nanocomposite films at 25 ˚C, the particles in a) and b) at interface.

In addition to AFM results, SEM results are represented in Figure 3.15 and the location of the NPs is releaved difference in PMMA and interphase of the polymers.

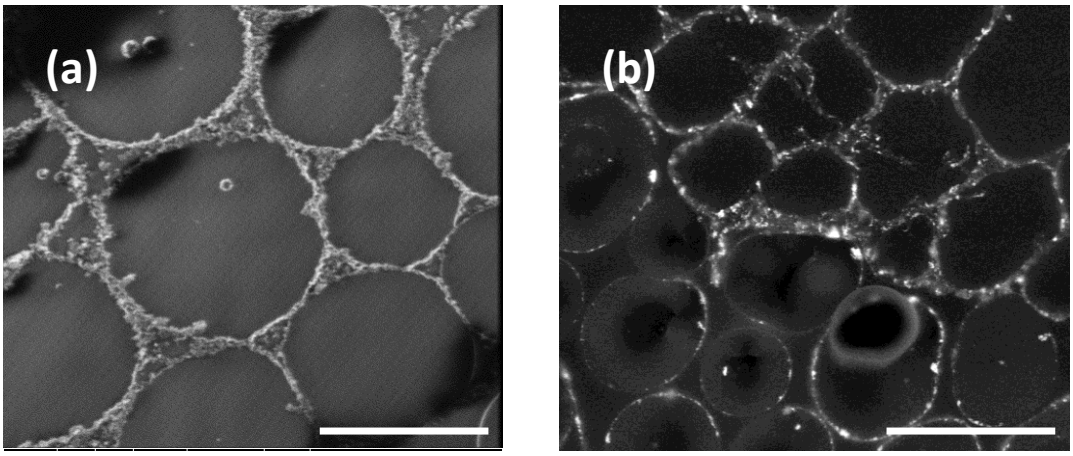

Figure 3.15. SEM images of nanocomposite films at 25 ˚C a) 4μm and b) 10 μm.

Size distribution of Ag/CTAB NPs in the polymer nanocomposites films were illustrated in Figure 3.16. The NPs located at interphase have the diameter 27 nm, calculated *d/L* ratio is 0.093. The larger Ag/CTAB NPs located at PMMA phase with the 90 nm diameter have the ratio 0.15. While smaller NPs with smaller *d/L* ratio load in interphase, larger NPs with larger *d/L* load in PMMA domain.

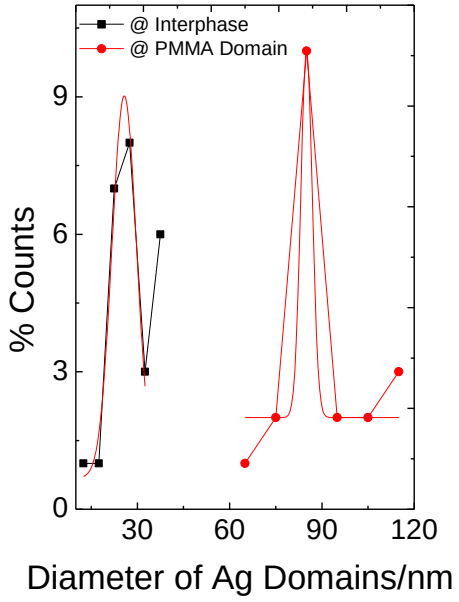

Figure 3.16. Size distribution of Ag/CTAB NPs at interphase and PMMA domains

As mentioned experimental part, Ag/CTAB-PS/PMMA nanocomposite films were annealed at 165 ˚C for 3 days. After annealing, the location of Ag/CTAB NPs is selectively loaded in PS domain as illustrated in Figure 3.17. The average diameter of Ag/CTAB NPs is approximately 69 nm and *d/L* ratio is 0.0437.

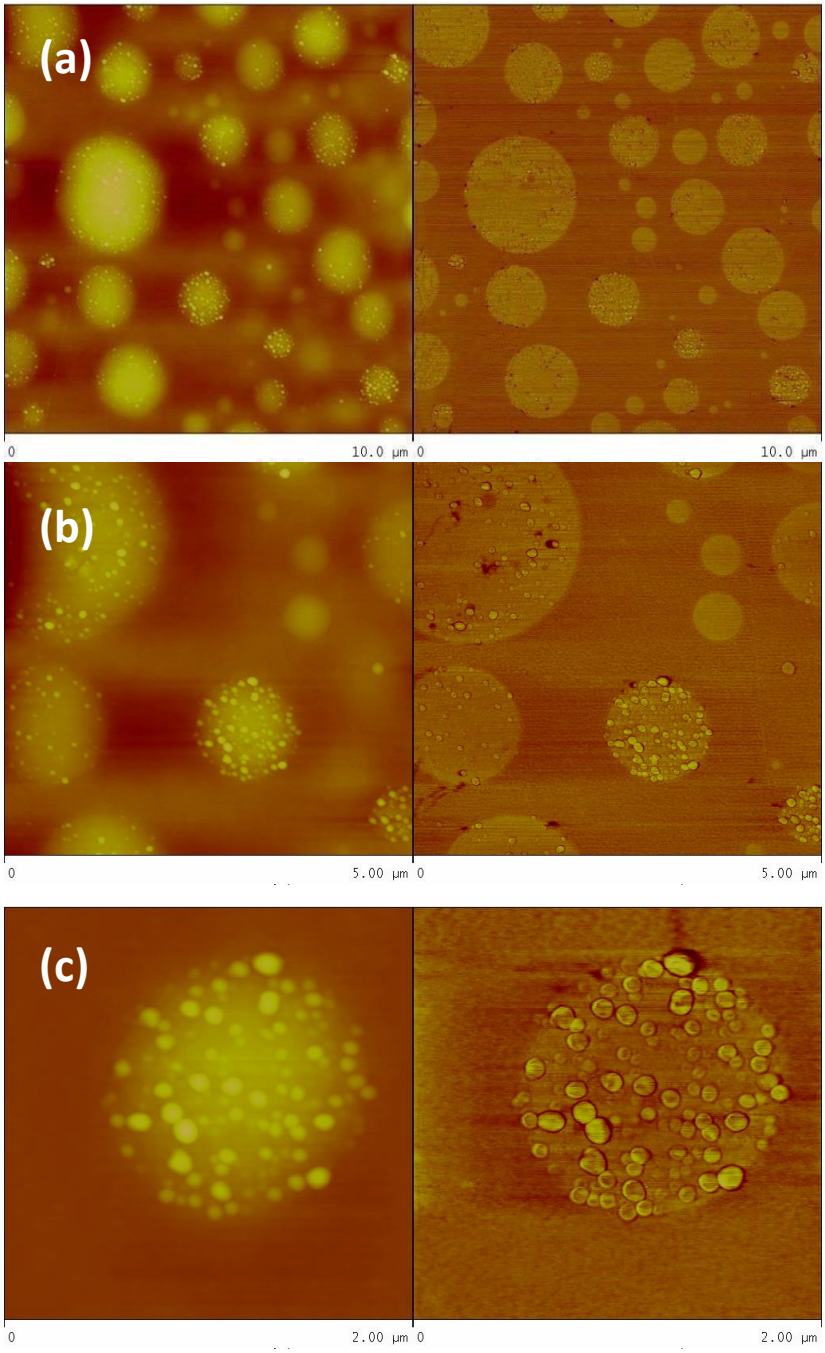

Figure 3.17. Tapping mode AFM images of Ag/CTAB-PS/ PMMA nanocomposite films at 165 ˚C.

The change in location of the NPs upon annealing can be explained with the change in surface tension of the PS and PMMA domain. In addition, wetting coefficients are calculated in table 3.3 for each case, the data was obtained by using the linear interpolation of the literature data and interfacial tension of CTAB was assumed as polyethylene due to same as aliphatic chain of CTAB molecule. As mentioned in previous part, if the wetting coefficient is between the -1 and 1, the particles locate interphase otherwise if it is greater than 1, the NPs place in the PS domain. (Syms, Yeatman, Bright, & Whitesides, 2003).

Table 3.3. Interfacial tension and wetting coefficient of the polymers

Temperature, °C	Interfacial Tension, mN/m			Wetting Coefficient
	PS/CTAB	PMMA/CTAB	PS/PMMA	
25	8.2[a]	11.1[b]	3.13[c]	0.93
165	5.4	9.3	1.38	2.79

a,b and c; (Wu, 1970)

To sum up the discussion on the size of PS domain in the case of composite preparation, (Figure 3.18), size of PS domains shows differences due to annealing and adding CTAB capped Ag NPs. The diameter of PS domains in polymer nanocomposite films without Ag/CTAB NPs is around 4.5 μm. After adding NPs at room temperature, the diameter is reduced to 400 nm. The reduction of PS domain size occurs most probably due to the surfactant effect of CTAB immobilized to the surface of Ag particles. Upon annealing the composite, the size of PS domains increases to 1.25 μm. Increase in temperature, the diffraction of PS domain is highly possible. The domains diffuse and coalescence forming larger PS domains compared to the domains develop in the presence of CTAB capped particles.

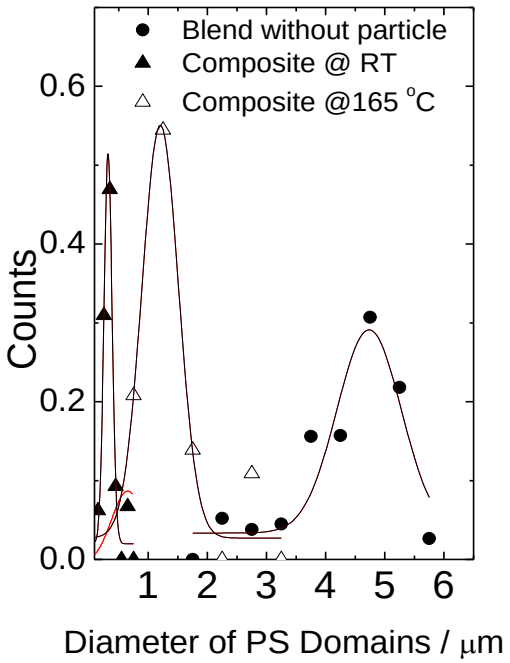

Figure 3.18. Size distribution of PS domains in polymer nanocomposite films.

TGA analysis result of the polymer nanocomposites at different temperatures is represented in Figure 3.19. In the analysis, temperature increases and mass of the sample as a function of temperature is recorded. First humidity and then organic part of the sample usually disappears. At high temperature after the degradation of polymers, inorganic content remains. The composite film prepared at room temperature provides 0.64 wt % at 600 ˚C. When this film is annealed at 165 ˚C, the remaining mass is 5.5 because humidity is already removed from the system and the fraction of Ag particles increases.

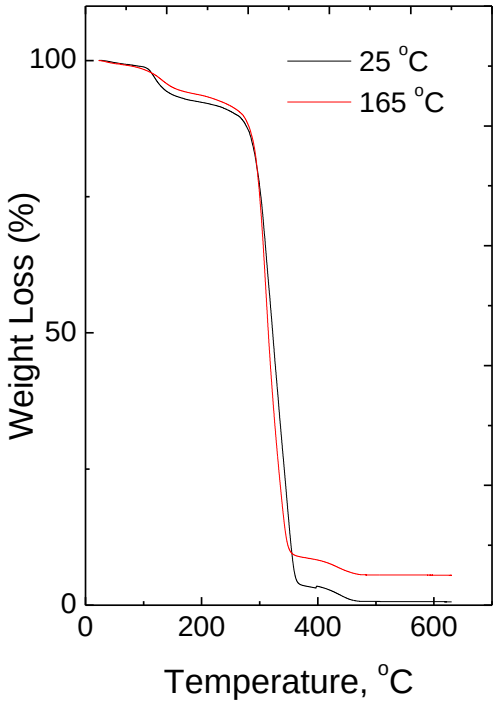

Figure 3.19. TGA result of the polymer nanocomposite films at 25 ˚C and 165 ˚C.

CHAPTER 4

CONCLUSIONS

We demonstrated that the composites of PS/PMMA blend and CTAB capped Ag nanoparticles were prepared. Ag nanoparticles were obtained by reduction of $AgNO_3$ via NaBH4. The particles are electrostatically stabilized due to the presence of BH_4(-) on the particle surface. Capping the particles by a cationic surfactant, CTAB makes them organophilic. The resulting particles were mixed with PS and PMMA in THF solution. The surface feature of the composite film and the location of the nanoparticles were figured put by AFM. The results state that both enthalpy and entropy are at play. Larger particles prefer to be present in PMMA. Because the ratio of particle domain size to the size of PS domain 0.15. This effect is purely entropic. Annealing of the composite films at 165 ˚C direct the particles and particle domains into PS domains. At this temperature, the surface tension of the Ag/CTAB particles gets close to the one of the PS domains. This effect, on the other hand, is enthalpic. The main conclusion of the results is that control over the location of the nanoparticles was successfully achieved. However, the development of any physical feature upon change of the location of the nanoparticles is not clarified in this study. There are two important parameters employed. First, the amount of particles was 0.7 % by weight. Second, the composition of the PS/PMMA blend was 1:1 in THF as 2.5% (w/v). The microstructure (phase separation of the polymer constituents and the location of the nanoparticles) can be studied in detail for future study. In consequence, controlling of the placement of the NPs in polymer blends as in our study gives point of view and development of novel nanomaterials.

REFERENCES

Chung, H.-j., Ohno, K., Fukuda, T., & Composto, R. J. (2005). Self-regulated structures in nanocomposites by directed nanoparticle assembly. *Nano letters, 5*(10), 1878-1882.

Morin, C., Ikeura-Sekiguchi, H., Tyliszczak, T., Cornelius, R., Brash, J., Hitchcock, A., . . . Winesett, D. (2001). X-ray spectromicroscopy of immiscible polymer blends: polystyrene–poly (methyl methacrylate). *Journal of Electron Spectroscopy and Related Phenomena, 121*(1), 203-224.

Mulfinger, L., Solomon, S. D., Bahadory, M., Jeyarajasingam, A. V., Rutkowsky, S. A., & Boritz, C. (2007). Synthesis and study of silver nanoparticles. *Journal of chemical education, 84*(2), 322.

Pötschke, P., Pegel, S., Claes, M., & Bonduel, D. (2008). A novel strategy to incorporate carbon nanotubes into thermoplastic matrices. *Macromolecular Rapid Communications, 29*(3), 244-251.

Prosycevas, I., Tamulevicius, S., & Guobiene, A. (2004). The surface properties of PS/PMMA blends nanostructured polymeric layers. *Thin solid films, 453*, 304-311.

Syms, R. R., Yeatman, E. M., Bright, V. M., & Whitesides, G. M. (2003). Surface tension-powered self-assembly of microstructures-the state-of-the-art. *Microelectromechanical Systems, Journal of, 12*(4), 387-417.

Ton-That, C., Shard, A., Teare, D., & Bradley, R. (2001). XPS and AFM surface studies of solvent-cast PS/PMMA blends. *Polymer, 42*(3), 1121-1129.

Bockstaller, M. R., Mickiewicz, R. A., & Thomas, E. L. (2005). Block copolymer nanocomposites: perspectives for tailored functional materials. *Advanced Materials, 17*(11), 1331-1349.

Chiu, J. J., Kim, B. J., Yi, G.-R., Bang, J., Kramer, E. J., & Pine, D. J. (2007). Distribution of nanoparticles in lamellar domains of block copolymers. *Macromolecules, 40*(9), 3361-3365.

Choi, O., Deng, K. K., Kim, N.-J., Ross Jr, L., Surampalli, R. Y., & Hu, Z. (2008). The inhibitory effects of silver nanoparticles, silver ions, and silver chloride colloids on microbial growth. *Water research, 42*(12), 3066-3074.

Chung, H.-j., Ohno, K., Fukuda, T., & Composto, R. J. (2005). Self-regulated structures in nanocomposites by directed nanoparticle assembly. *Nano letters, 5*(10), 1878-1882.

De Gryse, R., Depla, D., Poelman, D., Mahieu, S., Leroy, W., & Poelman, H. (2008). *Proceedings of ICTF 14 & RSD 2008*.

Demir, M. M., & Wegner, G. (2012). Challenges in the preparation of optical polymer composites with nanosized pigment particles: a review on recent efforts. *Macromolecular Materials and Engineering, 297*(9), 838-863.

Ha, M., Atallah, A., & Krishnamoorti, R. (2011). Effect of organically modified layered silicates on the morphology of symmetrical blends of polystyrene and poly (methyl methacrylate). *Polymer, 52*(25), 5890-5896.

He, G., Ginzburg, V. V., & Balazs, A. C. (2006). Determining the phase behavior of nanoparticle-filled binary blends. *Journal of Polymer Science Part B: Polymer Physics, 44*(17), 2389-2403.

Kao, J., Thorkelsson, K., Bai, P., Rancatore, B. J., & Xu, T. (2013). Toward functional nanocomposites: taking the best of nanoparticles, polymers, and small molecules. *Chemical Society Reviews, 42*(7), 2654-2678.

Morin, C., Ikeura-Sekiguchi, H., Tyliszczak, T., Cornelius, R., Brash, J., Hitchcock, A., . . . Winesett, D. (2001). X-ray spectromicroscopy of immiscible polymer blends: polystyrene–poly (methyl methacrylate). *Journal of Electron Spectroscopy and Related Phenomena, 121*(1), 203-224.

Mulfinger, L., Solomon, S. D., Bahadory, M., Jeyarajasingam, A. V., Rutkowsky, S. A., & Boritz, C. (2007). Synthesis and study of silver nanoparticles. *Journal of chemical education, 84*(2), 322.

Pötschke, P., Pegel, S., Claes, M., & Bonduel, D. (2008). A novel strategy to incorporate carbon nanotubes into thermoplastic matrices. *Macromolecular Rapid Communications, 29*(3), 244-251.

Prosycevas, I., Tamulevicius, S., & Guobiene, A. (2004). The surface properties of PS/PMMA blends nanostructured polymeric layers. *Thin solid films, 453*, 304-311.

Sui, Z., Chen, X., Wang, L., Xu, L., Zhuang, W., Chai, Y., & Yang, C. (2006). Capping effect of CTAB on positively charged Ag nanoparticles. *Physica E: Low-dimensional Systems and Nanostructures, 33*(2), 308-314.

Syms, R. R., Yeatman, E. M., Bright, V. M., & Whitesides, G. M. (2003). Surface tension-powered self-assembly of microstructures-the state-of-the-art. *Microelectromechanical Systems, Journal of, 12*(4), 387-417.

Tang, Y., Du, B., Yang, J., & Zhang, Y. (2006). Temperature effects on surface activity and application in oxidation of toluene derivatives of CTAB-SDS with KMnO4. *Journal of Chemical Sciences*, *118*(3), 281-285.

Thompson, R. B., Ginzburg, V. V., Matsen, M. W., & Balazs, A. C. (2001). Predicting the mesophases of copolymer-nanoparticle composites. *Science*, *292*(5526), 2469-2472.

Ton-That, C., Shard, A., Teare, D., & Bradley, R. (2001). XPS and AFM surface studies of solvent-cast PS/PMMA blends. *Polymer, 42*(3), 1121-1129.

Wu, S. (1970). Surface and interfacial tensions of polymer melts. II. Poly (methyl methacrylate), poly (n-butyl methacrylate), and polystyrene. *The Journal of Physical Chemistry*, *74*(3), 632-638.